Coupling PhreeqC with electro-diffusion tests for an accurate determination of the diffusion properties on cementitious materials

T. Sanchez, P. Henocq, O. Millet, A. Aït-Mokhtar

COUPLING PHREEQC WITH ELECTRO-DIFFUSION TESTS FOR AN ACCURATE DETERMINATION OF THE DIFFUSION PROPERTIES ON CEMENTITIOUS MATERIALS

T. Sanchez[1,3*], P. Henocq[2], O. Millet[3], and A. Aït-Mokhtar[3]

[1]Department of water and civil engineering, Laval University, Canada

[2]Andra, 1/7, rue Jean Monnet, Parc de la Croix-Blanche, 92298 Châtenay-Malabry Cedex

[3]LaSIE UMR CNRS 7356, University of La Rochelle, France

*Corresponding author. E-mail address: thomas.sanchez@gci.ulaval.ca

Abstract

An improved numerical method as regard with the widely used analytical approximation is presented for determining the transport properties from electro-diffusion tests. Based on the geochemical software PhreeqC, this study aims to better understand and quantify the part of each phenomenon in the diffusion process: (i) the geometrical material properties (as porosity and tortuosity); (ii) the chemical reactions between chloride ions and the cement solid phase; (iii) electro-capillarity effects (such as electrical double layer effects). Tests have been performed on CEM I hydrated cement pastes of different W/C ratio (0.35; 0.42 and 0.50) with different chloride concentrations (500 and 50 mol/m3). The results revealed a good accuracy on the chloride diffusion coefficients D_{E,Cl^-} given by the numerical model while having a weak set of main adjustable parameters. The large amount of experimental data collected during the tests increases the robustness of the model.

Keywords: Electro-Diffusion tests, Chloride, Cement materials, PhreeqC, Numerical model

1. Introduction

Many studies on chloride diffusion in cementitious materials are available in the civil engineering literature. The aim of these investigations is to quantify, in terms of durability, the degradation of reinforced concrete structures caused by chloride ions (marine or de-icing salt) [1–6] or radionuclides migration [7–9]. Most of them are experimental works and use a flux measure approach to determine the chloride diffusion coefficient [10–17]. To simplify, their models almost consider the same ratio between the effective diffusion coefficient $D_{E,i}$ (m²/s) for a ionic species i and its diffusion coefficient in free water $D_{W,i}$ (m²/s) [18,19]:

$$D_{E,i} = \emptyset G D_{W,i}. \quad (1)$$

Where $D_{E,i}$ depends on the diffusion coefficient in free water $D_{W,i}$, on the material porosity $\emptyset$, and another macroscopic geometrical parameter G. This last parameter represents the effect of the tortuosity, of the constrictivity, etc. and remains difficult to measure at the sample's scale.

Because of the huge complexity of the microstructure and chemistry of cementitious materials, most of the diffusive transport models in concrete are simplified. They only consider the diffusion of one ionic species the same time (as chloride ions) [20–22] and simplified chemical interactions as isotherms [23–27]. These isotherms help to simulate the chloride adsorption by the cementitious phases but do not consider other chemical reactions as calcium absorption by C-S-H gels (non-negligible for pH ≥ 10.5) [28] or sodium retention by C-S-H [29]. As well, chloride ions are bound by the cementitious material [24,30] but their adsorption is reduced by the sulfate concentration [31]. Some researches also observed that the quantity of sulfate absorbed by cementitious phases is more important than chloride one [32]. At last, the presence of chloride ions in the pore solution causes the precipitation of phases such as chloroaluminates [33].

More elaborated models hence consider the chloride interaction with the cement matrix [20,34,35] and/or electrocapillary effects like the electrical double layer (EDL) [5,6,36,37]. Some authors developed rigorous macroscopic transport models with homogenized methods to scale up the Nernst-Planck-Poisson-Boltzmann equation [38–43] from the microscopic scale (i.e. pore scale) to the macroscopic scale of the material sample. The averaging homogenization [44] is based on some simplifying assumptions and do not consider all the complexity of the microstructure (e.g. Samson et al. model [45]). The periodic homogenization [46,47] is mathematically more consistent and does not rely on supplementary simplifying assumptions (e.g. for clay minerals [48] and newly for concrete [49–53]). However, this approach remains formal and no convergence results have been obtained. More recently, homogenization by double-scale methods enables to obtain the homogenized model and the convergence at the same time [54–57]. Some results on properties of Nernst-Planck-Poisson and Nernst-Planck-Poisson-Boltzmann system may also be found in [42,43]. Inspiring of these last methods, the diffusion coefficients $D_{E,i}$ and $D_{W,i}$ can be related to a formation factor F_i [58] (instead of the geometrical parameter G in eq. (1)) :

$$D_{E,i} = F_i D_{W,i}. \quad (2)$$

Where F_i, also named scale-up factor, is in general interpreted as the path available for the diffusion of the ionic species i. Based on these analogies, a definition of F_i will be established for the present work as follows:

$$F_i = \emptyset G g_i \quad (3)$$

F_i includes the porosity $\emptyset$, geometrical microscopic effects G (such as tortuosity and constrictivity), and other microscopic effects g_i (such as the EDL).

However, all the mathematical models do not consider the ionic species activities and chemical reactions, such as the homogenous reactions that occur in the solution (complexation, inter-ions interaction) and the heterogeneous reactions with the material surface (sorption, solid phase

74 dissolution/precipitation) [59]. By diffusing into concrete, the ions modify the pore solution
75 chemical composition and disturb the local thermodynamic balance of the system. A series of
76 dissolution/precipitation reactions hence take place to restore the equilibrium state.
77 Other more elaborated multi-species transport models consider the diffusion of different species
78 coupled with chemical reactions [60,61] but do not allow the applying of an electrical field at
79 the material bounds to simulate accelerated diffusion test. Recently, the multi-species reactive
80 transport model PhreeqC was updated to simulate the application of an electrical potential all
81 over a chemical system [62]. This change has thus motivated this work which consists of
82 simulating electro-diffusion tests considering both multi-ionic diffusive transport and chemical
83 reactions.
84 Electro-diffusion tests were carried out on hydrated cement paste (HCP) samples with two
85 different chloride concentrations in upstream: 500 mol/m³ like in civil engineering applications,
86 simulating an average chloride concentration in seawater and 50 mol/m³ to tend the radionuclide
87 diffusive behaviour (see [63]). Section 2 introduces the experimental procedure of the material
88 characterisation and electro-diffusion and leaching tests as used in this work. The numerical
89 model on PhreeqC and its calibration are then presented in section 3. At last, the main results
90 obtained, in particular, the determination of effective diffusion coefficients are reported in
91 section 4.

92 ## 2. Experimental

93 ### 2.1. Materials and characterization

94 **Materials.** Experimental tests were carried out on CEM I hydrated cement pastes (CEM I
95 52.5N CE CPI2 NF called 'CEM I white') [NF EN 197-1 and NF P 15-318] with 0.35; 0.42 and
96 0.50 Water/Cement (W/C) ratio. Subsequently, these materials are noted CPI035, CPI042 and
97 CPI050 (for Cement Paste I). The specimens were stored in a basic solution with 83 mol/m³

KOH and 25 mol/m³ NaOH for 6 months at 20 °C and RH 100% to ensure the complete saturation of the material porosity. The saturation of samples was verified by immersion under vacuum in a desiccator for 24 hours. The first centimetres of each specimen from the surface was removed to avoid any edge effects and possible bleeding. Then, the specimens were cored and sawed in samples of 65 mm diameter and 10 mm thick.

Hydrated cement paste characterizations. Water porosities (Table 1) were measured in previous works [64]. The chemical composition of the pore solutions was measured equilibrating HCP powders in ultra-pure water with different Solid/Liquid ratio in g_{powder}/g_{water} (Table 1). All the concentrations were measured by ionic chromatography Metrohm 930 Compact IC Flex with around 10% accuracy (depending on the ion studied and the dilution used for analyses).

	CPI035	**CPI042**	**CPI050**
Water porosity	36%	40%	45%
Cl^- (mol/m³)	2.0	1.0	0.8
SO_4^{2-} (mol/m³)	0.21	0.22	0.18
Na^+ (mol/m³)	387	327	245
K^+ (mol/m³)	259	180	206

Table 1. Water porosity and pore solution composition of the three HCP [64]

2.2. Electro-diffusion tests

Electro-diffusion test modified procedure [64]**.** A saturated sample taken from the cure was resin-coated to let the diffusion be one-dimensional. It was placed between two cells (Figure 1): the upstream cell contains the tracer (chloride ions) in a basic solution composed of potassium hydroxide KOH and sodium hydroxide NaOH with concentrations given by the pore solution composition measurements (Table 1). The downstream cell contains only KOH and NaOH. During the test, the chloride diffusion through the material results from the concentration gradient between the two cells. To accelerate the process, a constant electrical field was applied

to the sample. The electrical field was fixed to respect a weak current value (below 50 mA). The current density passing through the sample and the chloride concentration in downstream were measured throughout the test. The ionic concentrations were then analyzed by ionic chromatography. Temperature and solution pH were also punctually measured during the test.

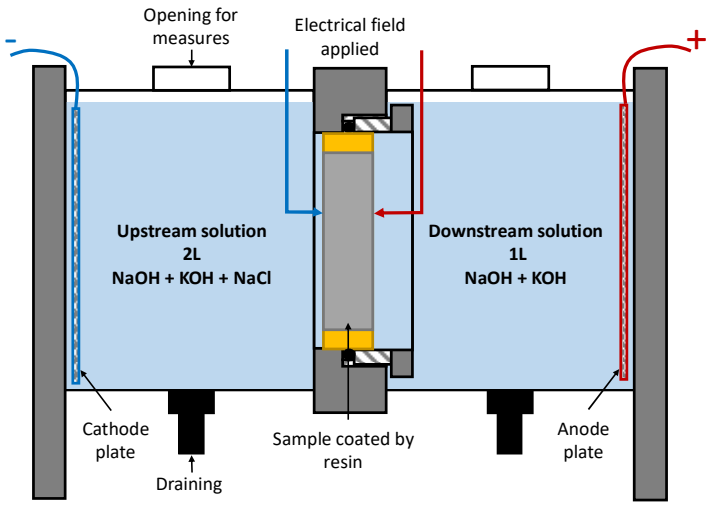

Figure 1. Schematic of electro-diffusion cells built [64]

Electro-diffusion test results. Tests were performed for the three HCP previously presented CPI035; CPI042 and CPI050 with two different chloride concentrations: 500 mol/m³ and 50 mol/m³. The test temperature is around 20-25°C. Other initial conditions (volume solutions, sample lengths and electrical field applied) are summarized in Table 2 and Table 3. The time evolution of the current and chloride concentration downstream are presented in Figure 2 and Figure 3.

Migration tests	Upstream/Downstream cell volume (L)	Sample Diameter x Length (mm)	Electrical field applied (V/m)
CPI050 1	2.17/1.17	63 x 11.3	14
CPI050 2	2.20/1.16	63 x 11.7	14
CPI042 1	2.10/1.21	63 x 11.8	12
CPI042 2	2.11/1.15	63 x 9.60	14
CPI035 1	2.12/1.15	63 x 10.3	21
CPI035 2	2.02/1.11	63 x 11.0	26

130 Table 2. Initial conditions summary for electro-diffusion tests with 500 mol/m3

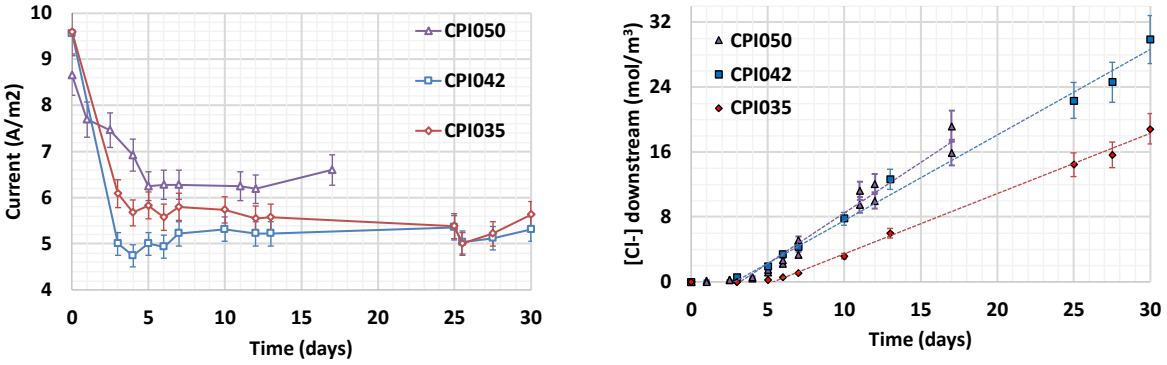

(a) (b)

131 Figure 2. Electro-diffusion tests with 500 mol/m^3 chloride in upstream: Time evolution of (a)

132 the current density and (b) the chloride concentration in downstream.

Migration tests	Upstream/Downstream cell volume (L)	Sample Diameter x Length (mm)	Electrical field applied (V/m)
CPI050 1	2.04/1.07	63 x 9.4	36
CPI050 2	1.89/1.02	63 x 9.5	37
CPI042 1	1.95/1.05	63 x 12.0	27
CPI042 2	1.99/1.07	63 x 12.0	27
CPI035 1	1.95/1.05	63 x 12.4	26
CPI035 2	1.85/0.90	63 x 12.8	27

133 Table 3 – Initial conditions summary for electro-diffusion tests with 50 mol/m3

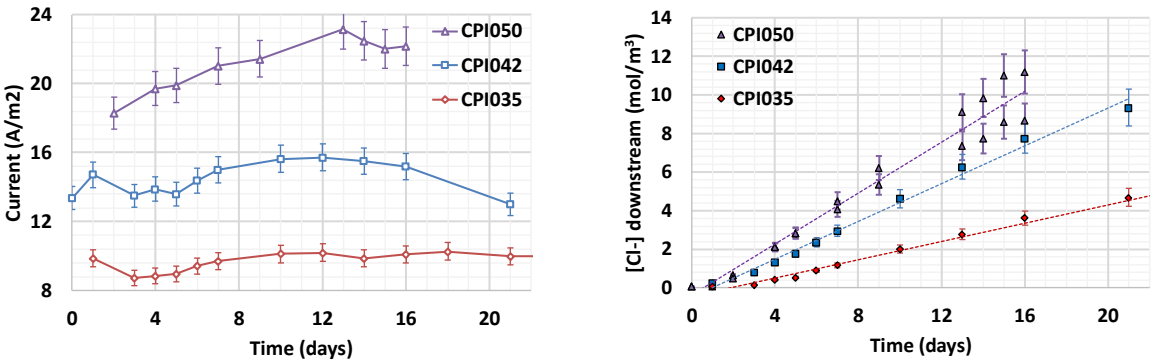

(a) (b)

Figure 3. Electro-diffusion tests with 50 mol/m^3 chloride in upstream: Time evolution of (a) the current density and (b) the chloride concentration in downstream.

2.3. Leaching tests

Semi-dynamic leaching test modified procedure. The leaching tests are liquid-solid extraction of a solid sample by an aqueous solution. Tests are based on the NF X31-210 French standard. They were performed to quantify the diffusion of major ionic species in the pore solution i.e. the alkaline species Na^+ and K^+. A HCP sample (same kind of electro-diffusion test sample) was coated on its circumference and on one face to obtain a one-direction ionic diffusion and simplify thereafter the numerical modelling (null flow condition at one end and constant flow at the only exposed surface). The HCP sample (around 33 ml) was put on a closed glass container and immersed in a volume of ultra-pure water (100 ml). This low volume of leaching solution allows observing small ionic concentrations with precision. However, it requires replacing each volume sampled (2.5 ml) by a new volume of ultra-pure water to conserve the sample immersed during all the tests (that qualifies the test as 'semi-dynamic leaching'). The leachate and the air above were constantly saturated with Argon using a sintered bubbler to prevent the leachate carbonation (Figure 4). The leaching container has different orifices to regularly measure pH and sample the solution for alkali concentration analyses. The test usually lasts some weeks to one month.

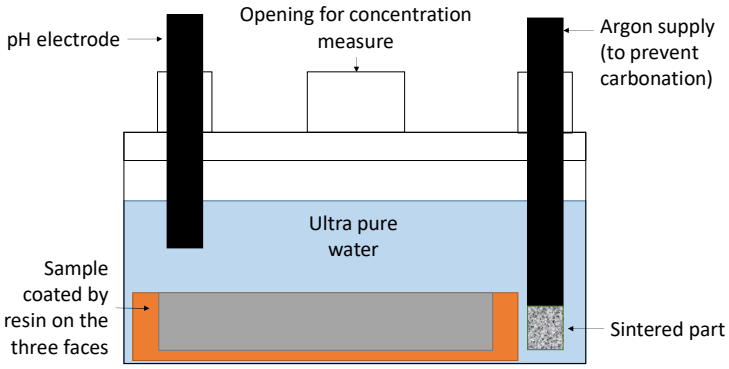

Figure 4. Schematic view of the modified leaching test on a hydrated cement paste sample

Leaching test results. An example of a leaching test with a CPI050 hydrated cement paste sample is presented in Figure 5. The material was put in 100 ml of ultra-pure, the temperature was around 19.5°C and pH stabilized very quickly around 12.5. The evolutions of Na^+ and K^+ concentrations in the leachate solution can be observed during the 11-day tests. The two alkaline species (Na^+ and K^+) have similar diffusion and concentration values.

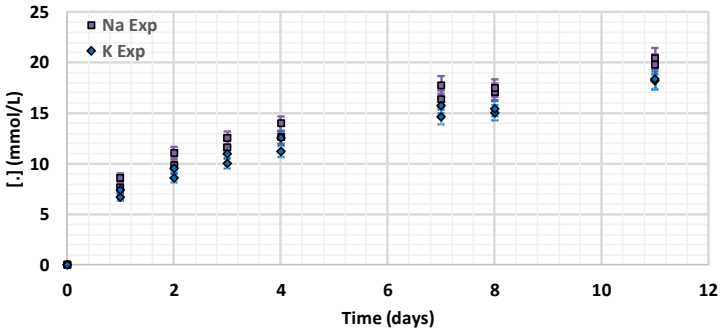

Figure 5. Leaching test on CPI050: alkali concentration evolution with time in the leachate solution

3. Numerical part

3.1. Numerical model and assumptions

PhreeqC is a freeware developed in C/C++ by D. Parkhurst and C.A.J. Appelo and used in many common industrial and academic applications [65,66]. This software allows simulating classical 1D macroscopic transport equations coupled to reactive processes with a rich chemical

database (e.g. [67]). PhreeqC simulate, with a chemical reaction module, the dissolution and precipitation of material solid phases, the oxidation-reduction reactions at the electrodes and the balance between an aqueous phase and the atmosphere surrounding (pure phases, solid solutions, exchange surfaces…). PhreeqC requires a consistent thermodynamic database including in our case cementitious minerals and radionuclides. The numerical model is solved using an explicit finite element scheme which is faster than an implicit one but can be unstable if the initial conditions are not physically compatible or if the space step is too large (not respecting Von Neumann criterion [68]).

Code improvements were recently made to consider the application of an electrical field applied at the material boundaries to simulate an electro-diffusion test (version 3.3.12 Ampere). The modifications were validated on electro-diffusion tests and the numerical solution was compared with the Krabbenhoft analytic approach [62].

In this study, we consider that the ionic diffusion takes place under isothermal conditions; the HCP are constantly saturated, and the samples have a sufficiently large thickness (1 cm) to consider their microstructured equivalent to a representative one. Moreover, the diffusion is assumed to be unidimensional (with sample coating).

3.2. Numerical resolution

The sample is spatially discretized in n cells where both chemical reactions and 1D diffusive transport take place. The diffusive transport at the macroscopic scale follows the macroscopic Nernst-Planck equation [40,41]:

$$\frac{\partial c_i}{\partial t} = -\frac{\partial J_i}{\partial x} - \frac{\partial q_i}{\partial t} \tag{4}$$

where J_i represents the ionic flux (mol/m²/s) defined by:

$$J_i = -D_{E,i}\left(\frac{\partial c_i}{\partial x} + c_i \frac{\partial \ln \gamma_i}{\partial x} + \frac{z_i c_i F}{RT}\frac{\partial \psi}{\partial x}\right). \tag{5}$$

188 Where γ_i denotes the ionic activity of ion i (-), ψ the induced potential (V), z_i the valence of
189 ion i (-), F the Faraday constant (C/mol), R the perfect gas constant (J/K/mol), T the
190 temperature (K). The chemical fixation q_i (mol/m³) is defined by the concentration $c_{s,i}$ (mol/kg)
191 of an ionic species bound to the surface of the material modelled [69]:

$$q_i = \frac{c_{s,i}\,\rho_b}{\emptyset_i} \tag{6}$$

192 where ρ_b is the density of the free area (kg/m³) and $\emptyset_i$ the accessible porosity (-). In the
193 numerical model proposed, the concentration $c_i(t + \Delta t)$ of a species i at time step $(t + \Delta t)$
194 depends on $c_i(t)$ respecting an explicit time scheme (Figure 6).

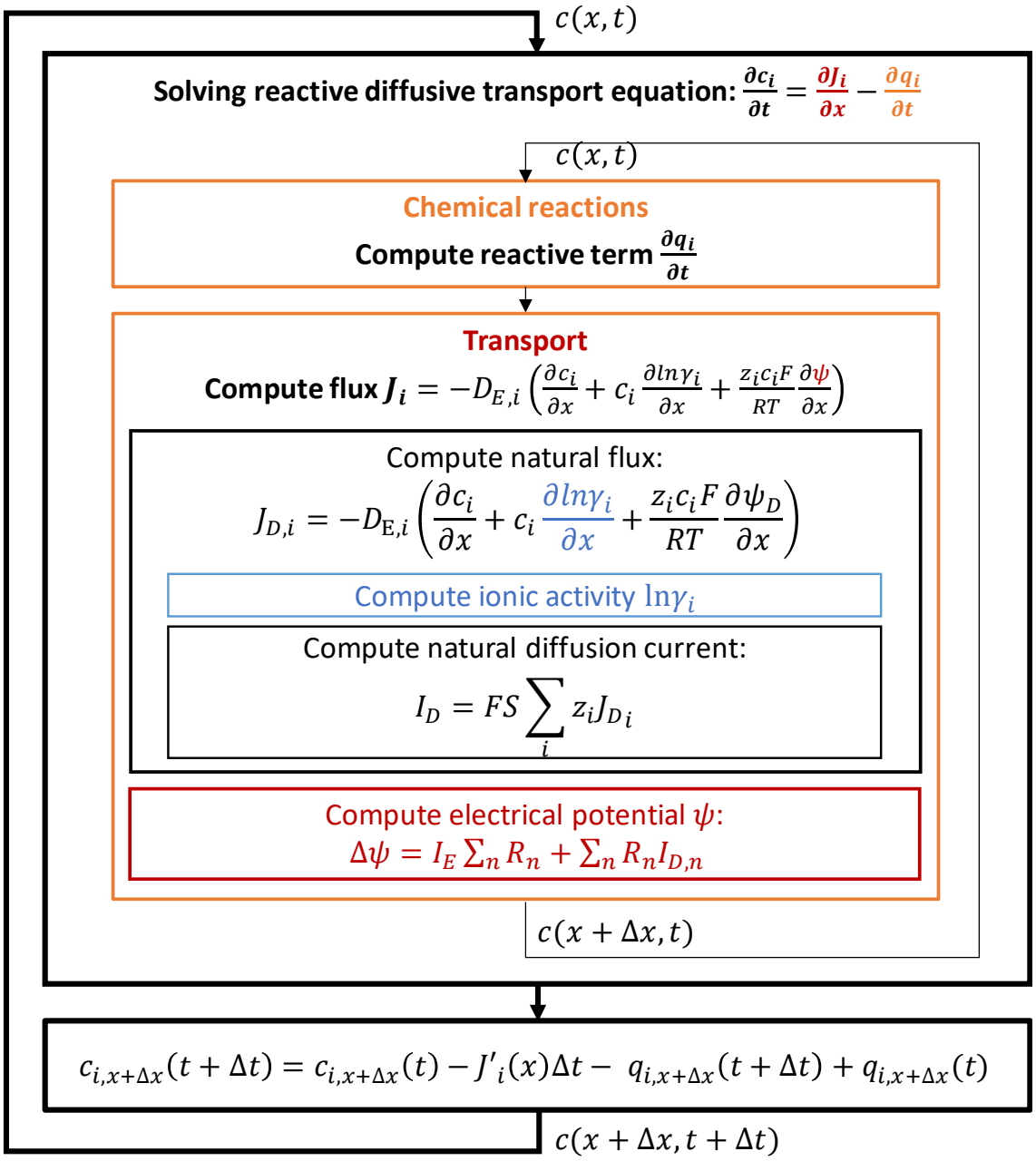

Figure 6 – Algorithm for solving electro-diffusion transport with chemical reactions

Chemical reactions. The computation of the reactive term $\frac{\partial q_i}{\partial t}$ is performed with a decoupled PhreeqC chemical reaction module [70] which is not detailed in this paper. Chemical reactions and their associated kinetics are solved with Range-Kutta method [71]. The chemical reaction time step is automatically adapted to ensure the convergence of the computation algorithm of $\frac{\partial q_i}{\partial t}$. In general, it is much more smaller than the time step used for solving the transport

equation, due to the different time scales involved. The iterative Newton-Raphson method [72] allows finding an optimal chemical state (it may also use an optimization method if chemical reactions are not linearly independent [73]).

Natural diffusion equation. The ionic activity $\ln\gamma_i$ is calculated using Truesdell-Jones equation for the majority ions [74], Debye-Huckel ones for the minority ions [75] or Davis ones by default when nothing else is specified [76]. The flux term $\frac{\partial J_i}{\partial x}$ is solved for a natural diffusion using the open current hypothesis considering that the electrical current due to natural diffusion is null [48,77]. $\frac{\partial J_i}{\partial x}$ is computed by a centered spatial scheme [78] and the current induced by natural diffusion in each cell j is hence obtained from:

$$I_{D,j} = FS\left(\sum_i z_i J_{D,i}\right)_j. \tag{7}$$

where $J_{D,i}$ denotes the current due to natural diffusion only.

Electro-diffusion equation. Potential gradient $\nabla\psi_j$ at the bounds of a cell j (length Δx) is classically computed from:

$$\nabla\psi_j = \frac{(\psi_j - \psi_{j-1})}{\Delta x}. \tag{8}$$

It is important to notice that ψ includes both the natural potential and the applied electrical potential $(\psi_n - \psi_0)$ across the entire sample (Figure 7). The total current $I_{tot,j}$ flowing through a cell j hence comes both from the natural diffusion $I_{D,j}$ (calculated previously in (7)) and the application of an external electrical potential $I_{E,j}$. The total current I_{tot} is assumed to be the same for all cells [79]. This hypothesis considers that there is no accumulation of charges in the material (by an electrical analogy, no capacitor in the circuit):

$$I_{tot} = I_{D,1} + I_{E,1} = \cdots = I_{D,n} + I_{E,n}. \tag{9}$$

Each cell can, therefore, be represented as two resistances in parallel (defined by Ohm's law [80]): $R_{D,j} = (\psi_j - \psi_{j-1})/I_{D,j}$ and $R_{E,j} = (\psi_j - \psi_{j-1})/I_{E,j}$ which depends on the concentration of species in the pore solution of cell j and on their diffusion coefficients [81,82].

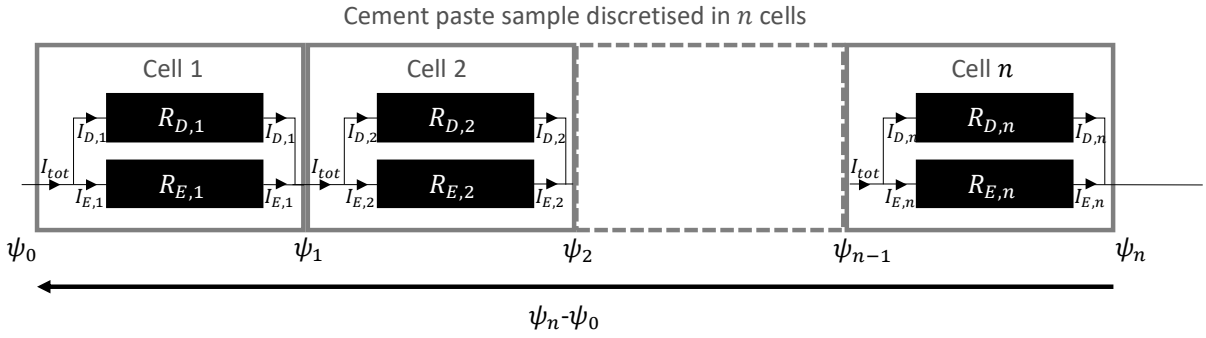

Figure 7. Schematic representation of the material sample composed of n cells subjected to an applied electrical field

Assuming that the material is homogeneously saturated, the difference in electrical potential is evenly distributed in the cells. The potential difference across each cell $(\psi_j - \psi_{j-1})$ is calculated using $I_{E,j}$. For the first cell [80]:

$$I_{E,1} = \frac{\psi_1 - \psi_0}{R_1} = \frac{(\psi_n - \psi_0)/n}{R_1}. \quad (10)$$

According to Kirchhoff's law [83], we can calculate the current I_E in cell 2, 3… and by recurrence on the potential difference across j:

$$\psi_j - \psi_{j-1} = R_j\left(I_{tot} - I_{D,j}\right) \quad (11)$$

3.3. Test of numerical models

Effective diffusion coefficient $D_{E,i}$. In the expression of the ionic flux J_i (equation (5)), the effective diffusion coefficient $D_{E,i}$ depends on the formation factor $F_i = \emptyset P_{Current} P_{[i]}$ (see Eqs. (2) and (3)). Whereas the porosity $\emptyset$ is measured by water, the numerical parameters $P_{Current}$ and $P_{[i]}$ have been introduced in PhreeqC to represent the influence of the sample microstructure geometry G and other microscopic effects g_i on a ionic species i:

- With the electro-diffusion tests, $P_{Current}$ and $P_{[Cl^-]}$ were both fitted with the evolutions of the current and the chloride concentration in downstream. The current evolution represents the ionic flux sum thus $P_{Current}$ represents the geometrical effects common to all ions in the system. As for $P_{[Cl^-]}$, it takes into account only the specific effects that influence the chloride transport (not other species).
- With the leaching tests, as $P_{Current}$ is determined by the electro-diffusion test on the same type of material, the alkalis concentration curves are fitted with their specific numerical parameters $P_{[Na^+]}$ and $P_{[K^+]}$.

Chemical reactions. PhreeqC uses 'phreeqc.dat' database validated and tested [84]. For this work, the main components of cementitious materials were added through the routine PHASES: portlandite, gypsum, calcite and CSH gels providing from the Thermochimie database developped by the consortium Andra/Ondraf-Niras/RWM (https://www.thermochimie-tdb.com/) [85–87]; ettringite and monosulfoaluminate from CEMDATA07 [88]; Kuzel and Friedel salts dissolution/precipitation [34] from Thermochimie. For each ionic species, the diffusion coefficients in free water $D_{L,i}$ is informed (–dw) and, for this work, contains also the numerical parameters $P_{[i]}$.

Electro-diffusion test initial conditions. The upstream solution is represented by a solution named SOLUTION 0 in PhreeqC (Figure 8) where its volume (-water in the SOLUTION 0 routine) and the average temperature measured during the test and initial concentrations are informed. Then it is possible to compute pH according to the species present (using charge routine) and to prevent non-physical compatibility because of uncertainties on pH and concentration measures. The oxidation-reduction reactions at the electrodes are considered with routine EQUILIBRIUM_PHASES 0.

```
SOLUTION 0 # Upstream solution
 -water 2.12          # Volume (L)
 -temperature 22.2    # Temperature en (°C)
 -units mmol/kgw
 pH 13.40 charge
 Cl 50.95             # Initial concentration (mmol/L)
 Na 69.79             # Initial concentration (mmol/L)
 K 124.81             # Initial concentration (mmol/L)
END

EQUILIBRIUM_PHASES 0 # Electrode
  H2(g) 0 0      # Saturation index and gas molality (mol)
END
```

Figure 8 – Representation of the upstream cell and electrode in the PhreeqC code

The sample material is discretized into several cells (25 for the example of Figure 9). Each cell contains both the initial pore solution composition (SOLUTION 1-25) and the solid phase (EQUILIBRIUM_PHASES 1-25 and SOLID_SOLUTIONS 1-25). The main species in solution were measured (see pore solution characterization in 2.1) while the minor species were computed by PhreeqC equilibrating the solution with the solid phases (portlandite and monosulfoaluminate for calcium and aluminium, respectively). The cementitious phases are considered initially stable (their saturation index equals zero). Each pore sub-solution is considered to be in contact with a sub-solid phase containing the major phases (C-S-H, portlandite…). The range of initial molar content values of the cementitious phases respect those observed for this kind of material. Then it is possible to slightly adjust the monosulfoaluminate and ettringite molalities reacting with chloride ions. Reaction between chloride and monosulfoaluminate AFm to form Friedel's salt or Kuzel's salt [34] can be characterized by a solid solution (SOLID_SOLUTIONS 1-25) as defined below. Dissolution/precipitation phenomenon or ionic exchange can hence be considered.

```
SOLUTION 1-25 # The 25 pore sub-solutions
 -water 8.09e-4          # Sub-solutions volume (L) : V_Solution 1-25 = Ø V_Sample / 25
 -temperature 22.2       # Température (°C)
 -units mmol/kgw
 pH 13.5 charge
 Na 23                   # Initial concentration (mmol/L)
 Ca 0.03 Portlandite     # Initial concentration (mmol/L) adjusted by portlandite molality
 K 52
 S(6) 0.22
 Al 0.18 Monosulfoaluminate
 Cl 2.0
END
```

276

```
EQUILIBRIUM_PHASES 1-25 # The 25 sub solid phase of the material
CSH1.6 0 1e-3              # Saturation index and initial molality
CSH1.42 0 0                # Phase not initially present
CSH1.06 0 0
CSH0.7 0 0
Portlandite 0 1e-3
Ettringite 0 4e-5
Monosulfoaluminate 0 15e-5
END
SOLID_SOLUTIONS 1-25 # Solid solutions present in the material
cement
 -comp Monosulfoaluminate 0   # Initial molality (mol)
 -comp Friedel-salt 0
 -comp Kuzel-salt 0

END
```

277

278

279 Figure 9 - Representation of the sample (pore solution, solid phase and solid solutions) in the
280 PhreeqC code

281 Similar to the upstream cell, a SOLUTION 26 routine represents the downstream cell. The
282 applied electrical potential applied ($\psi_{25} - \psi_0$), remaining constant during the electro-diffusion
283 test, is indicated by the function -potential (Figure 10).

```
EQUILIBRIUM_PHASES 26 # Electrode
 O2(g) 0 0     # Saturation index and gas molality (mol)
END
SOLUTION 26 # Downstream solution
 -water 1.1215        # Volume (L)
 -temperature 22.2    # Temperature (°C)
 -units mmol/kgw
 pH 13.40 charge
 Na 62.01             # Initial concentration (mmol/L)
 K 156.59
 -potential 13.65     # Constant electrical potential applied (V) (ψ25 − ψ0)
END
```

Figure 10 - Representation of the downstream cell and electrode in the PhreeqC code

Multi-species diffusive transport model. The multi-species transport takes place in the 25 cells whose length (-lengths) is specified in the TRANSPORT routine (Figure 11). The material boundary conditions (-boundary_conditions) consider the concentration evolution at upstream and downstream (flux boundary also known as first type or Dirichlet boundary). The natural transport is only due to diffusion (specified in the line -flow_direction) as the sample is saturated (no advection). PhreeqC simulates a multi-species diffusion with the function -multi_d. For this research need, it contains implicitly the numerical parameter $P_{Current}$ (Figure 11 in appendix).

```
TRANSPORT
 -cells 25                              # Number of cells
 -lengths 0.432e-3                      # Length of each cell (m)
 -boundary_conditions flux flux         # Flux conditions at the material bounds
 -flow_direction diffusion_only         # Only diffusion for transport
 -multi_d true 1e-9 0.007 0.0 1 false   # Multi-species diffusion with:
                                        # D_W,i by default / P_Current / Not Used
 -time_step 1 hour 5                    # Time step: 1 hour divided in 5 sub time steps
 -shifts 24                             # Number of time step before the first sampling
END
```

Figure 11 – Multi-species diffusion transport in the PhreeqC code

The time step and the number of time steps (-shifts) are also given in routine TRANSPORT. The simulation is divided into several sub-simulations corresponding to the electro-diffusion test duration between each solution sampling. When the upstream and downstream cells are sampled for concentration measurements, their volume decrease during the test: that is considered in PhreeqC.

Leaching test model specificity. The leaching test model is similar to electro-diffusion one except for the following points: The 100 ml leaching solution is represented in SOLUTION 0 routine by an ultra-pure water solution; the regular replacement of the solution sampled with ultra-pure water is considered; a closed boundary condition represents the resin-coated surface; a low electrical current (-fix_current in routine TRANSPORT) initiates the natural diffusion (to have a non-null potential at first cells).

4. Coupling PhreeqC and experimental tests

4.1. Calibration on HCP model CPI050 with 500 mol/m³ tests

Step (a). First, the global parameter $P_{Current}$ is adjusted using the current evolution with time. During the transient regime, the current decreased due to the leaching of alkaline species from the pore solution of the sample to the upstream cell. Then, the current became stable and reached a value that can be adjusted from experiments of electro-diffusion tests with the parameter $P_{Current}$ (Figure 12a$_1$). On the steady-state, the current tends to increase because alkaline species in the downstream solution migrate through the material to upstream under the effect of the electrical field applied. The slope of this curve is then adjusted by the numerical parameters $P_{[Na^+]}$ and $P_{[K^+]}$. Moreover, as the concentration measurements during the electro-diffusion tests do not allow obtaining a precise value for $P_{[Na^+]}$ and $P_{[K^+]}$ (because of the high Na^+ and K^+ concentrations used), these two parameters were determined with the PhreeqC simulation of leaching tests on the same type of HCP (Figure 12a$_2$). As the leaching simulation consider the replacement of the solution samples, it involves the curve discontinuities as observed in Figure 12a$_2$.

Step (b). The sulfate leaching from the HCP in the downstream cell during the electro-diffusion test (as sulfate are not initially present upstream and downstream) is fitted to provide additional information on sulfate-containing phases. Sulfate leaching is only influenced by the global parameter $P_{Current}$ and the initial molar content of monosulfoaluminate (AFm) and ettringite (AFt). The sulfate curve highlights two different slopes controlled by the AFm phase, and then by the AFt phase (Figure 12b). As $P_{Current}$ has been adjusted previously with current, the initial content of AFm and AFt permit fitting the two slopes. The ettringite saturation index was also adjusted to force its precipitation that seems to be accelerated by the electrical field applied or the high concentration of chloride used in the electro-diffusion test. The consistency of the AFm

content used in the code can be verifiecd with the timelap in the chloride curve : the delay at the test beginning is mainly due to the adsorption of chloride ions by monosulfoaluminate (Figure 12c).

Step (c). Finally, the chloride parameter $P_{[Cl^-]}$ was adjusted to reproduce the steady state of chloride experimental curve (Figure 12c) and consider other effects (in particular charge effects or EDL) affecting the chloride diffusion that are not included in the global parameter $P_{Current}$. $P_{[Cl^-]}$ fitting does not influence significantly the current and sulfate behaviour. The correct fit of the 3 curves is checked one last time. Then, we deduce by different fitting, that the chloride diffusion coefficient can vary about $D_{E,Cl^-} = \emptyset P_{current} P_{[Cl^-]} D_{W,Cl} =$ (7.9-8.9) x10^{-12} m²/s while respecting the current, sulfate and chloride curves.

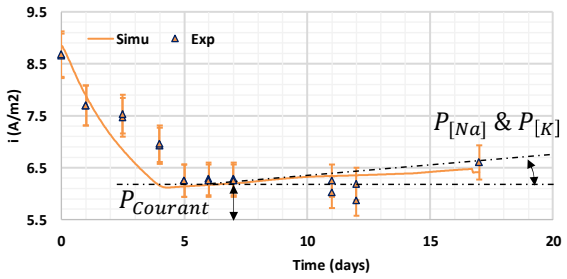

(a1) Current adjustment with $P_{Current}$, $P_{[Na^+]}$and $P_{[K^+]}$

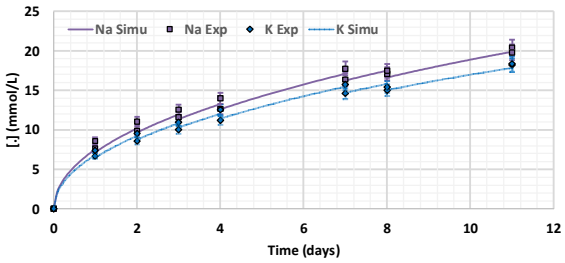

(a2) Determination of $P_{[Na^+]}$and $P_{[K^+]}$ with a leaching test simulation on CPI050

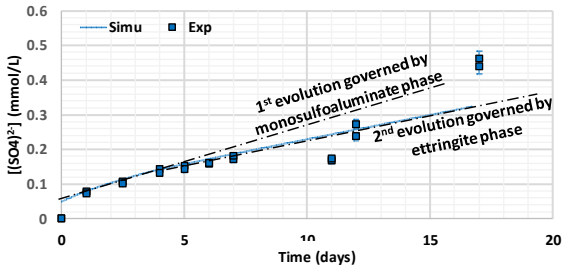

(b) Sulfate behavior adjustment with ettringite molar content

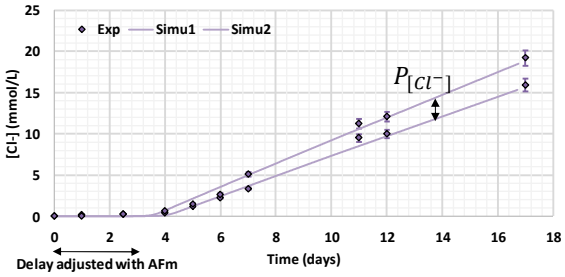

(c) Chloride adjustment with Afm content and P_{Cl^-}

Figure 12. Calibration of an electro-diffusion test on CPI050 with 500 mol/m³ of chlorides in upstream

4.2. Numerical model sensitivity

The numerical model sensitivity was evaluated on CPI050 with 50 mol/m³ of chloride in the upstream cell (Figure 13) according to the main parameters influencing the chloride diffusion coefficient (porosity, pore solution alkalinity, chloride timelap and the number of measured points). The objective is to identify the code adjustment parameter presenting experimental uncertainties and to quantify the consequences on the diffusion coefficient $D_{E,Cl^- PhreeqC}$.

(a) The porosity is one of the determining parameters in the diffusion process. It is measured with water at ± 1% and considered in the sub-pore solution volumes of the PhreeqC model. If there is an error of ± 5% in the porosity informed in PhreeqC, there is no difference in the sulfate concentration curve. However, the chloride and current curves (Figure 13a) vary significantly since the porosity $\emptyset$ is included in the diffusion coefficient ($D_{E,i} = \emptyset P_{Current} P_{[i]} D_{W,i}$). The numerical parameter $P_{Current}$ can be adjusted to counterbalance the error of the porosity measurements without having a direct consequence on the value of $D_{E,i}$. Indeed, in the code, the product $\emptyset P_{Current}$ remains constant. Some sensitivity studies in the literature corroborate these results [89].

(b) The pore solution alkalinity is an indicator of the ionic species that have the most influence on the current evolution. Hydroxide concentrations in the pore solution were measured by pH meter at ±0.2. These uncertainties can induce important changes in chloride, sulfate and current curves (Figure 13b). It could be possible to readjust the curves modifying $P_{Current}$ but it would induce a non-negligible error of 13% on the diffusion coefficient D_{E,Cl^-}. The consistency of the pore solution pH is rather checked corroborating the leaching test results which are carried out on the same type of material (with the same numerical parameter $P_{Current}$). The leaching tests permit to obtain a good approximation of the initial alkalis concentration in the pore solution and of their diffusion coefficients, based on the evolution of their leaching. Thus, coupling the

368 two numerical models (electro-diffusion and leaching tests) allows to cross the experimental
369 results and refine the meaurements of pH and concentrations in the pore solution and the alkali
370 transport parameters ($P_{Current}$, P_{Na^+}, P_{K^+}).
371 (c) The chloride timelap in downstream depends not only on the geometry of the material but
372 also on chloride reactions with solid phases. Friedel and Kuzel's salts are assumed not to be
373 present initially, the only adjustable parameter that influence chloride timelap in downstream is
374 the initial monosulfoaluminate AFm molar content (Figure 13c). As it was not measured in this
375 work, the AFm molar content can be evaluated at ± 5 mol/m³ based on literature data. However,
376 the numerical simulations allow increasing the accuracy to ± 1 mol/m³ on the AFm molar
377 content by jointly fitting the curves of chloride and sulfate in downstream. The accuracy on the
378 AFm molar content thus mainly depends on the frequency of measurements at the test
379 beginning (during the unsteady state).
380 (d) For a high chloride concentration in upstream (500 mol/m³), the steady-state regime was
381 reached very quickly then it was easy to reproduce the linear chloride curve and obtain an
382 accurate diffusion coefficient D_{E,Cl^-}. With a lower concentration such as 50 mol/m³, it can be
383 more difficult to fit the chloride curve if there are not enough measure points for chloride
384 concentration. The error on D_{E,Cl^-} according to the number of measuring points fitted in the
385 numerical model was evaluated by adjusting the two main parameters influencing chloride
386 evolution, i.e. AFm molar content for the chloride timelap and $P_{[Cl^-]}$ for curve slopes (Figure
387 13d). It reveals that it is necessary to have at least six non-null measured points on the chloride
388 curve. However, the uncertainties on D_{E,Cl^-} slightly increase after too long a time may be due
389 to the upstream solution carbonation or the material degradation caused by the electrical field
390 applied.

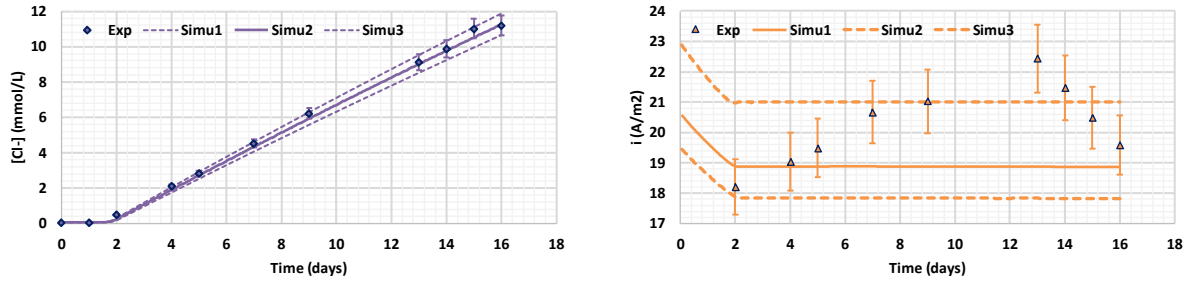

(a) Porosity influence on chloride and current curves. Porosity varying ± 5%

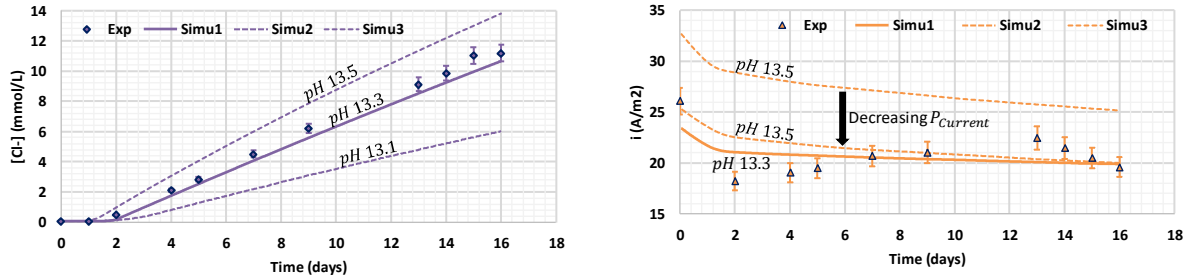

(b) pH influence on chloride and current curves. pH varying ±0.2

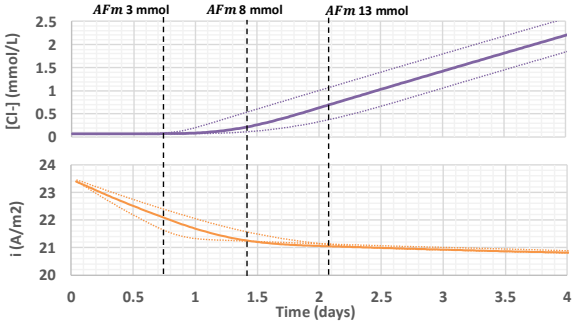

(c) AFm influence on chloride and current curves (±5 mmol)

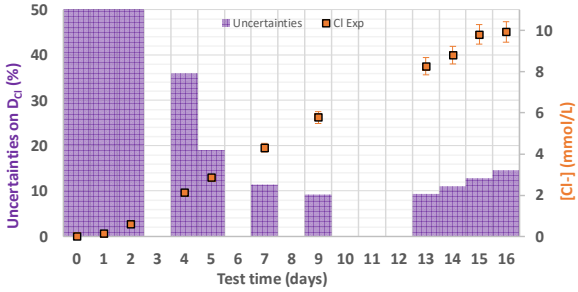

(d) Number of measures influence on chloride curve

Figure 13. Numerical model sensitivity: examples on CPI050 electro-diffusion test with 50 mol/m³ chloride in upstream

As a conclusion of the sensitivity study, the minimal uncertainties in the chloride diffusion coefficient are estimated at about 10% (for 7 measured points). Using an simplified method by measuring the flux in the steady-state regime [64], the sensitivity for the same case (CPI050 with 50 mol/m³) is estimated at approximately 18%.

4.3. Adaptation of the CPI050 model to CPI042/CPI035

CPI042/CPI035 models with 500 mol/m³ of chloride. The previous numerical model CPI050 was adapted for the two hydrated cement pastes CPI042 and CPI035. To this end, the numerical

parameters $P_{Current}$ and $P_{[Cl^-]}$ were slightly adjusted to well fit the current and chloride curves, and the saturation index for ettringite was adjusted to reproduce the sulfate curve. The chloride diffusion coefficient $D_{E,Cl^-\ PhreeqC}$ for the three HCP with 500 mol/m³ of chloride in upstream deduced from the simulations are presented in Table 4.

	CPI050	**CPI042**	**CPI035**
$\boldsymbol{D_{E,Cl^-\ PhreeqC}}$ **(10^{-12} m²/s)**	8.4 (±0.5)	6.8 (±0.4)	2.9 (±0.1)
$\boldsymbol{D_{E,Cl^-\ Simpl}}$ **(10^{-12} m²/s) [64]**	8.1 (±0.8)	4.7 (±0.6)	2.7 (±0.3)

Table 4 – Effective diffusion coefficient for chloride obtained with PhreeqC and from expression [64] on CPI050, CPI042 and CPI035 with 500 mol/m³ of chloride in upstream

The chloride diffusion coefficients obtained with PhreeqC are in the average of the experimental values for a CEM I HCP of the same ratio (between 0.35 and 0.5) [90]. We observe a difference in the chloride diffusive behaviour within the three materials which nevertheless have a closed microstructure. Indeed, W/C ratios, water and mercury porosities are not so far apart and the chloride diffusion coefficients obtained are of the same order of magnitude. Those results are coherent: chloride diffusion is slower when the HCP contains less water and less porosity to diffuse. These values are also coherent with those calculated by a simplified method measuring the flux $D_{E,Cl^-\ Simpl}$ [64] on the same electro-diffusion tests. Moreover, the values obtained with PhreeqC are two times more precise than the simplified expression $D_{E,Cl^-\ Simpl}$ commonly used (uncertainties of 5% and 12% resp.). This can be explained by more numerous experimental data used for the PhreeqC method by reproducing the current, sulfate and chloride behaviours.

The successive reversion between experiments and simulations allows refining the model and leads to a more realistic and reliable tool.

CPI050/CPI042/CPI035 with 50 mol/m³ of chloride. Using the same parameters $P_{Current}^{CPI050}$, $P_{Current}^{CPI042}$ and $P_{Current}^{CPI035}$ obtained from electro-diffusion tests with 500 mol/m³ of chlorides,

numerical current curves well fit the experiments. Indeed, the materials tested and their geometries were similar. However, the ettringite dissolution in the numerical model was not forced to fit the sulfate curve, as done in the three previous models. The AFt dissolution cannot be provoked by the electrical potential as they were similar in 50 and 500 mol/m³ tests. We can hence deduce that the acceleration of the ettringite dissolution observed in the 500 mol/m³ tests should be caused by the high chloride concentration in upstream inducing a stronger ionic strength than with only 50 mol/m³ of chloride in upstream. Then, for the three 50 mol/m³ tests, the ettringite index saturation in the numerical models are set to zero. As well, AFt and AFm phases have the same molar content as in 500 mol/m³ models; $P_{[Cl^-]}^{CPI050}$ for 50 mol/m³ test is the same as for 500 mol/m³ test; and $P_{[Cl^-]}^{CPI042}$ and $P_{[Cl^-]}^{CPI035}$ are slightly adjusted to fit the chloride curves. Thus, the chloride diffusion coefficients $D_{E,Cl^-\,PhreeqC}$ deduced from the simulations are similar to those obtained from the 500 mol/m³ tests in view of uncertainties (Table 5). The uncertainties on the chloride diffusion coefficient $D_{E,Cl^-\,PhreeqC}$ for 50 mol/m³ tests are slightly greater than with 500 mol/m³ tests (uncertainties of 5% and 9% resp.). However, it is still possible to observe differences in behaviour between the three HCP when reducing the chloride concentration in upstream. As previously, the values calculated for the simplified diffusion coefficient $D_{E,Cl^-\,Simpl}$ are not accurate enough to observe any difference between the two hydrated cement pastes CPI050 and CPI042 (uncertainties of arround 31%). The numerical model has the advantage to correct some experimental data uncertainties (such as the material boundary conditions or temperature test fluctuation) as it is based on multiple experimental curves and numerous measured points. The PhreeqC model is, therefore, more precise to use with a lower concentration of chlorides.

	CPI050	CPI042	CPI035
$D_{E,Cl^- PhreeqC}$ (10^{-12} m²/s)	9.9 (±1.0)	7.0 (±0.6)	2.2 (±0.2)
$D_{E,Cl^- Simpl}$ (10^{-12} m²/s) [64]	7.3 (±1.3)	4.8 (±1.4)	1.9 (±0.9)

Table 5 – Effective diffusion coefficient of chloride obtained with PhreeqC and simplified expression on CPI050, CPI042 and CPI035 with 50 mol/m³ chloride in upstream

Formation factors for the 500 and 50 mol/m³ tests. F_{Cl^-} was calculated using a chloride diffusion coefficient in free water D_{W,Cl^-}= 2.032x10^{-9} m²/s. For the HCP with the highest liquid volume (i.e. CPI050 and CPI042), accounting the uncertainties, F_{Cl^-} appeared similar regardless of the initial chloride concentration in upstream: $F_{Cl^-,500}^{CPI050} = F_{Cl^-,50}^{CPI050}$ and $F_{Cl^-,500}^{CPI042} = F_{Cl^-,50}^{CPI042}$ (Figure 14). However, we can observe a significant difference for CPI035 that seems not to be due to measurement uncertainties: $F_{Cl^-}^{CPI035}$ was smaller when the chloride ions were less concentrated upstream ($F_{Cl^-,50}^{CPI042} < F_{Cl^-,500}^{CPI042}$).

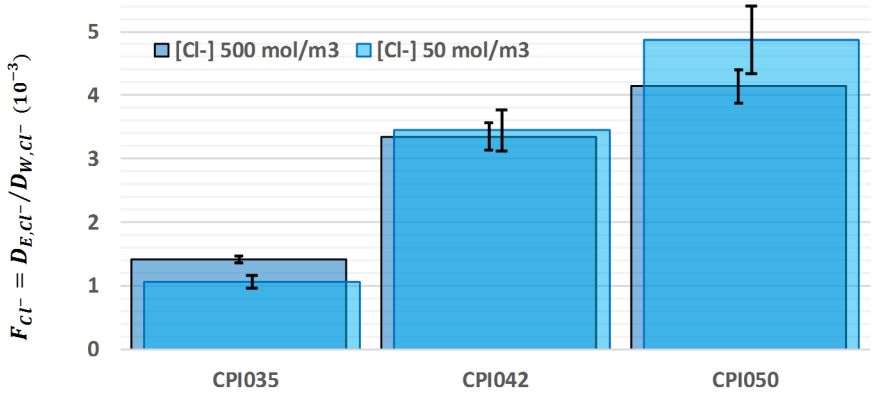

Figure 14. Formation factors calculated for the three HCP with two different chloride concentrations in upstream

A lower porosity could involve microscopic phenomenon slowing down the chloride diffusion. This phenomenon could be mainly related to the electrocapillary effects such as the C-S-H surface charge [36]. Indeed, the influence of the electrical double layer (EDL), directly linked to the Debye length, is inversely proportional to the ionic concentration of the pore solution and

460 the pore size [91]. That could explain why EDL effects are negligible for the highest chloride
461 concentration at 500 mol/m³ and for CPI050 and CPI042 which have high water volumes and
462 porosities. Based on equation (3) and the observation in Figure 14, as the microstructure ($\emptyset$ and
463 G) is similar for a same type of material regardless the chloride concentration in upstream, the
464 following results can be deduced:

$$\begin{matrix} g_{Cl^-,50}^{CPI050} \cong g_{Cl^-,500}^{CPI050} \\ g_{Cl^-,50}^{CPI042} \cong g_{Cl^-,500}^{CPI042} \\ g_{Cl^-,50}^{CPI035} < g_{Cl^-,500}^{CPI035} \end{matrix}. \quad (12)$$

465 Moreover, as no microscopic effects seems to be present for high chloride concentration and
466 thus high ionic strength (i.e. $g_{Cl^-,500}^{CPI050} \cong g_{Cl^-,500}^{CPI042} \cong g_{Cl^-,500}^{CPI035} \cong 1$), it is possible to conclude
467 from (12) that there is also no microscopic effects on CPI042 and CPI050 for lower chloride
468 concentrations:

$$g_{Cl^-,50}^{CPI050} \cong g_{Cl^-,50}^{CPI042} \cong 1 \quad (13)$$

469 A different conclusion is nevertheless highlighted for the least porous HCP (CPI035) when
470 chloride ions are less concentrated:

$$g_{Cl^-,50}^{CPI035} < 1. \quad (14)$$

471 That underlines the need to redefine the definition of the formation factor distinguishing
472 macroscopic and microscopic geometrical effects and including expressly the EDL effects.

473 **5. Conclusions**

474 The numerical model developed on PhreeqC allowed simulating accurately electro-diffusion
475 tests on cementitious materials considering both the diffusive transport and chemical reactions.
476 Leaching test simulations completed the electro-diffusion tests one as they had a common
477 physical-chemical basis and same numerical parameters for the sample (dimensions,
478 microstructure complexity, cementitious phases, pore solution composition, etc.).

The sensitivity analyse revealed a weak set of main parameters in the numerical model ($P_{Current}$ for global geometrical effects and $P_{[Cl^-]}$ for geometrical effects influencing only chloride diffusion) and a good accuracy of the measurement of D_{E,Cl^-} (±10%). The AFm molar content could also be a numerical parameter if it is not measured. $P_{Current}$ and $P_{[Cl^-]}$ are equivalent to the tortuosity parameter that can be found in most transport models. The large amount of experimental data, available for a given type of sample and used to calibrate the numerical model, increases its robustness. Successive back and forth between experiments and simulations make it possible to refine the modeling of physic-chemistry with PhreeqC.

First calibrated on hydrated cement pastes with electro-diffusion tests at 500 mol/m³ of chloride in upstream (civil engineering conditions), the numerical modelling allowed to accurately compare chloride diffusive behaviour (uncertainties of 5% with the model compared to 9% with a simplified equation). It also allowed separating the influence of physical and chemical effects on the chloride transport.

Decreasing the chloride concentration in the upstream cell, uncertainties on the chloride diffusion coefficients using a simplified equation became arround 31%. This did not permit to differentiate the materials studied. However, with the numerical model, a difference in behaviour between the three HCP of different W/C ratio could be observe (and uncertainties were only about 9% using the numerical model). With a lower chloride concentration in upstream and an HCP with very low porosity, some microscopic effects slowing down the chloride diffusion seemed to appear. Further studies are then required to verify this result. Electro-diffusion tests and simulations have to be carried out with other tracers on HCP: cationic species (such as Cs+ and Li+) to observe the influence of the ionic charge and neutral species (such as HTO) which are not influenced by electrochemical effects.

6. Acknowledgement

This research has been funded by Andra. The authors acknowledge the technical support of LaSIE Laboratory with Jean-Francois Meusnier (building electro-diffusion cells), Bruno Peraudeau (designing assistance for leaching tests) and Anthony Gélicus (chromatography assistance). The authors also acknowledge A. Hamami for his collaboration on experimental studies and C.A.J. Appelo for his collaboration on the PhreeqC adding (electrical field applied).

7. References

[1] J.-P. Bigas, La diffusion des ions chlore dans les mortiers, PhD Thesis, Toulouse, INSA, 1994.
[2] P. Locoge, M. Massat, J.P. Ollivier, C. Richet, Ion diffusion in microcracked concrete, Cem. Concr. Res. 22 (1992) 431–438. https://doi.org/10/drwcgq.
[3] C.L. Page, N.R. Short, A. El Tarras, Diffusion of chloride ions in hardened cement pastes, Cem. Concr. Res. 11 (1981) 395–406. https://doi.org/10/d78r43.
[4] O. Amiri, A. Aït-Mokhtar, A. Seigneurin, A complement to the discussion of A. Xu and S. Chandra about the paper "Calculation of chloride coefficient diffusion in concrete from ionic migration measurements" by C. Andrade, Cem. Concr. Res. 27 (1997) 951–957.
[5] O. Amiri, A. Aıt-Mokhtar, P. Dumargue, G. Touchard, Electrochemical modelling of chloride migration in cement based materials: Part I: Theoretical basis at microscopic scale, Electrochimica Acta. 46 (2001) 1267–1275. https://doi.org/10/ctqq4f.
[6] O. Amiri, A. Aït-Mokhtar, P. Dumargue, G. Touchard, Electrochemical modelling of chlorides migration in cement based materials. Part II: Experimental study—calculation of chlorides flux, Electrochimica Acta. 46 (2001) 3589–3597. https://doi.org/10/fmn9wm.
[7] Z. Bajja, W. Dridi, B. Larbi, P. Le Bescop, The validity of the formation factor concept from through-out diffusion tests on Portland cement mortars, Cem. Concr. Compos. 63 (2015) 76–83.
[8] Y. Albinsson, K. Andersson, S. Börjesson, B. Allard, Diffusion of radionuclides in concrete and concrete-bentonite systems, J. Contam. Hydrol. 21 (1996) 189–200.
[9] A. Atkinson, A.K. Nickerson, Diffusion and sorption of cesium, strontium, and iodine in water-saturated cement, Nucl. Technol. 81 (1988) 100–113.
[10] D.C. Grahame, Fiftieth Anniversary: Mathematical Theory of the Faradaic Admittance Pseudocapacity and Polarization Resistance, J. Electrochem. Soc. 99 (1952) 370C–385C.
[11] A. Ait-Mokhtar, O. Amiri, O. Poupard, P. Dumargue, A new method for determination of chloride flux in cement-based materials from chronoamperometry, Cem. Concr. Compos. 26 (2004) 339–345. https://doi.org/10/bhm5cd.
[12] C. Andrade, Calculation of chloride diffusion coefficients in concrete from ionic migration measurements, Cem. Concr. Res. 23 (1993) 724–742.
[13] L.O. Nilsson, E. Poulsen, P. Sandberg, H.E. Sørensen, O. Klinghoffer, HETEK, chloride penetration into concrete, state-of-the-art, transport processes, corrosion initiation, test methods and prediction models, Den. ISSNISBN. (1996) 0909–4288.

[14] L. Tang, Chloride transport in concrete-measurement and prediction, PhD thesis, 1996.
[15] J.-M. Loche, A. Ammar, P. Dumargue, Influence of the migration of chloride ions on the electrochemical impedance spectroscopy of mortar paste, Cem. Concr. Res. 35 (2005) 1797–1803. https://doi.org/10/crdd8z.
[16] T. Zhang, Chloride diffusivity in concrete and its measurement from steady state migration testing, Norwegian University of Science and Technology, 1997.
[17] L.O. Nilsson, E. Poulsen, P. Sandberg, H.E. Sørensen, O. Klinghoffer, HETEK, chloride penetration into concrete, state-of-the-art, transport processes, corrosion initiation, test methods and prediction models, Den. ISSNISBN. (1996) 0909–4288.
[18] E. Samson, G. Lemaire, J. Marchand, J.J. Beaudoin, Modeling chemical activity effects in strong ionic solutions, Comput. Mater. Sci. 15 (1999) 285–294.
[19] K.A. Snyder, The relationship between the formation factor and the diffusion coefficient of porous materials saturated with concentrated electrolytes: theoretical and experimental considerations, Concr. Sci. Eng. 3 (2001) 216–224.
[20] O. Truc, J.P. Ollivier, M. Carcassès, A new way for determining the chloride diffusion coefficient in concrete from steady state migration test, Cem. Concr. Res. 30 (2000) 217–226. https://doi.org/10/cs546q.
[21] E.J. Hansen, V.E. Saouma, Numerical simulation of reinforced concrete deterioration-Part I: Chloride diffusion, ACI Mater. J. 96 (1999) 173–180.
[22] S. Swaddiwudhipong, S.F. Wong, T.H. Wee, S.L. Lee, Chloride ingress in partially and fully saturated concretes, Concr. Sci. Eng. 2 (2000) 17–31.
[23] B. Martın-Pérez, Service life modelling of RC higway structures exposed to chlorides, Univ. Tor. Tor. (1999).
[24] T. Luping, L.-O. Nilsson, Chloride binding capacity and binding isotherms of OPC pastes and mortars, Cem. Concr. Res. 23 (1993) 247–253.
[25] J. Arsenault, Etude des mécanismes de transport des ions chlore dans le béton en vue de la mise au point d'un essai de migration, 1999.
[26] O. Francy, Modélisation de la pénétration des ions chlorures dans les mortiers partiellement saturés en eau, PhD Thesis, Toulouse 3, 1998.
[27] O. Amiri, H. Friedmann, A. Aït-Mokhtar, Modelling of chloride-binding isotherm by multi-species approach in cement mortars submitted to migration test, Mag. Concr. Res. 58 (2006) 93–99.
[28] P. Henocq, Modélisation des interactions ioniques à la surface des Silicates de Calcium Hydratés, (2005) 245.
[29] H. Viallis-Terrisse, Interaction des Silicates de Calcium Hydratés, principaux constituants du ciment, avec les chlorures d'alcalins. Analogie avec les argiles, These Univ. Bourgogne. (2000).
[30] A. Delagrave, Mecanismes de penetration des ions chlore et de degradation des systemes cimentaires normaux et a haute performance., (1997).
[31] R. Barbarulo, Comportement des matériaux cimentaires: actions des sulfates et de la température, LMT-ENS Cachan Fr. Thèse Dr. (2002).
[32] Y. Maltais, J. Marchand, P. Henocq, T. Zhang, J. Duchesne, Ionic interactions in cement-based materials: importance of physical and chemical interactions in presence of chloride or sulfate ions, Mater. Sci. Concr. VII Am. Ceram. Soc. USA. (2004).
[33] H. Zibara, Binding of external chlorides by cement pastes, PhD Thesis, National Library of Canada= Bibliothèque nationale du Canada, 2001.
[34] F. Barberon, V. Baroghel-Bouny, H. Zanni, B. Bresson, J.-B. d'Espinose de la Caillerie, L. Malosse, Z. Gan, Interactions between chloride and cement-paste materials, Magn. Reson. Imaging. 23 (2005) 267–272. https://doi.org/10/dk2d8v.

[35] V. Baroghel-Bouny, X. Wang, M. Thiery, M. Saillio, F. Barberon, Prediction of chloride binding isotherms of cementitious materials by analytical model or numerical inverse analysis, Cem. Concr. Res. 42 (2012) 1207–1224. https://doi.org/10/gc5pk5.
[36] S. Chatterji, M. Kawamura, Electrical double layer, ion transport and reactions in hardened cement paste, Cem. Concr. Res. 22 (1992) 774–782.
[37] P.T. Nguyen, O. Amiri, Study of electrical double layer effect on chloride transport in unsaturated concrete, Constr. Build. Mater. 50 (2014) 492–498. https://doi.org/10/gc5pk2.
[38] R.J. Hunter, Foundation of Colloidal, Oxford University Press, 2001.
[39] J.D. Jackson, Electrodynamics, Wiley Online Library, 1975.
[40] W. Nernst, Die elektromotorische wirksamkeit der jonen, Z. Für Phys. Chem. 4 (1889) 129–181.
[41] M. Planck, Zur Theorie der Elektrizitätserregung in Elektrolyten, Z. Für Phys. 94 (1935) 469–472.
[42] G. Gagneux, O. Millet, General Properties of the Nernst-Planck-Poisson-Boltzmann System Describing Electrocapillary Effects in Porous Media, J. Elast. 117 (2014) 213–230. https://doi.org/10/f6k9hf.
[43] G. Gagneux, O. Millet, A survey on properties of Nernst–Planck–Poisson system. application to ionic transport in porous media, Appl. Math. Model. 40 (2016) 846–858.
[44] S. Whitaker, Simultaneous heat, mass, and momentum transfer in porous media: a theory of drying, in: Adv. Heat Transf., Elsevier, 1977: pp. 119–203.
[45] E. Samson, J. Marchand, Modeling the transport of ions in unsaturated cement-based materials, Comput. Struct. 85 (2007) 1740–1756. https://doi.org/10/bhgmm3.
[46] J.-L. Auriault, J. Lewandowska, Diffusion/adsorption/advection macrotransport in soils, Eur. J. Mech. Solids. 15 (1996) 681–704.
[47] E. Sánchez-Palencia, Non-homogeneous media and vibration theory, Lect. Notes Phys. 127 (1980).
[48] C. Moyne, M.A. Murad, A two-scale model for coupled electro-chemo-mechanical phenomena and onsager's reciprocity relations in expansive clays: I homogenization analysis, Transp. Porous Media. 62 (2006) 333–380.
[49] K. Bourbatache, O. Millet, A. Aït-Mokhtar, Multi-scale periodic homogenization of ionic transfer in cementitious materials, Heat Mass Transf. 52 (2016) 1489–1499.
[50] K. Bourbatache, O. Millet, A. Aït-Mokhtar, O. Amiri, Modeling the Chlorides Transport in Cementitious Materials By Periodic Homogenization, Transp. Porous Media. 94 (2012) 437–459. https://doi.org/10.1007/s11242-012-0013-1.
[51] K. Bourbatache, O. Millet, A. Aït-Mokhtar, Ionic transfer in charged porous media. Periodic homogenization and parametric study on 2D microstructures, Int. J. Heat Mass Transf. 55 (2012) 5979–5991. https://doi.org/10/f38szn.
[52] K. Bourbatache, O. Millet, A. Aït-Mokhtar, O. Amiri, Chloride transfer in cement-based materials. Part 1. Theoretical basis and modelling, Int. J. Numer. Anal. Methods Geomech. 37 (2013) 1614–1627.
[53] K. Bourbatache, O. Millet, A. Aït-Mokhtar, O. Amiri, Chloride transfer in cement-based materials. Part 2. Experimental study and numerical simulations, Int. J. Numer. Anal. Methods Geomech. 37 (2013) 1628–1641.
[54] G. Allaire, Homogenization and two-scale convergence, SIAM J. Math. Anal. 23 (1992) 1482–1518.
[55] G. Gagneux, O. Millet, Homogenization of the Nernst-Planck-Poisson System by Two-Scale Convergence, J. Elast. 114 (2014) 69–84. https://doi.org/10/gc4phj.
[56] U. Hornung, Homogenization and porous media, Springer Science & Business Media, 2012.

[57] G. Nguetseng, A general convergence result for a functional related to the theory of homogenization, SIAM J. Math. Anal. 20 (1989) 608–623.
[58] G. Arliguie, H. Hornain, Grandeurs associées à la Durabilité des Bétons, Paris Presse L'Ecole Natl. Ponts Chaussées. (2007).
[59] J. Rubin, Transport of reacting solutes in porous media: Relation between mathematical nature of problem formulation and chemical nature of reactions, Water Resour. Res. 19 (1983) 1231–1252. https://doi.org/10/fgqjzf.
[60] D. Planel, Les effets couplés de la précipitation d'espèces secondaires sur le comportement mécanique et la dégradation des bétons, PhD Thesis, PhD thesis, University of Marne La Vallée, 2002.
[61] O. Truc, Prediction of chloride penetration into saturated concrete - multi-species approach, Chalmers Univ, Göteborg, 2000.
[62] C.A.J. Appelo, Solute transport solved with the Nernst-Planck equation for concrete pores with 'free' water and a double layer, Cem. Concr. Res. 101 (2017) 102–113. https://doi.org/10/gc4phg.
[63] T. Sanchez, A. Ait-Mokhtar, P. Henocq, A. Hamami,, O. Millet, Development of An Accelerated Electro-diffusion Test for Radionuclides Through Cementitious Materials, Cem Concr Res. (2019).
[64] T. Sanchez, A. Ait-Mokhtar, Henocq, Pierre, Hamami, Ameur El Amine, O. Millet, Development of An Accelerated Migration Test for Radionuclides Through Cementitious Materials, Cem. Concr. Res. (2018).
[65] D.L. Parkhurst, C.A.J. Appelo, Description of input and examples for PHREEQC version 3–A computer program for speciation, batch-reaction, one-dimensional transport, and inverse geochemical calculations, (2013).
[66] D.L. Parkhurst, C.A.J. Appelo, User's guide to PHREEQC (Version 2): A computer program for speciation, batch-reaction, one-dimensional transport, and inverse geochemical calculations, (1999).
[67] C.A.J. Appelo, L.R. Van Loon, P. Wersin, Multicomponent diffusion of a suite of tracers (HTO, Cl, Br, I, Na, Sr, Cs) in a single sample of Opalinus Clay, Geochim. Cosmochim. Acta. 74 (2010) 1201–1219. https://doi.org/10.1016/j.gca.2009.11.013.
[68] J.G. Charney, R. Fjörtoft, J. von Neumann, Numerical integration of the barotropic vorticity equation, Tellus. 2 (1950) 237–254.
[69] C.D. Shackelford, D.E. Daniel, Diffusion in saturated soil. I: Background, J. Geotech. Eng. 117 (1991) 467–484.
[70] G.T. Yeh, V.S. Tripathi, A critical evaluation of recent developments in hydrogeochemical transport models of reactive multichemical components, Water Resour. Res. 25 (1989) 93–108.
[71] E. Fehlberg, Low-order classical Runge-Kutta formulas with stepsize control and their application to some heat transfer problems, (1969).
[72] J. Raphson, Analysis aequationum universalis seu ad aequationes algebraicas resolvendas methodus generalis, & expedita, ex nova infinitarum serierum methodo, deducta ac demonstrata, typis Tho. Braddyll, prostant venales apud Johannem Taylor, 1702.
[73] I. Barrodale, F.D.K. Roberts, Algorithm 552: Solution of the Constrained I 1 Linear Approximation Problem [F4], ACM Trans. Math. Softw. TOMS. 6 (1980) 231–235.
[74] A.H. Truesdell, B.F. Jones, WATEQ, a computer program for calculating chemical equilibria of natural waters, J Res US Geol Surv. 2 (1974) 233–248.
[75] P. Debye, E. Hückel, On the theory of electrolytes. I. Freezing point depression and related phenomena, Collect. Pap. Peter JW Debye. (1954) 217–263.
[76] C.W. Davies, T. Shedlovsky, Ion association, J. Electrochem. Soc. 111 (1964) 85C–86C.

[77] C.A.J. Appelo, P. Wersin, Multicomponent Diffusion Modeling in Clay Systems with Application to the Diffusion of Tritium, Iodide, and Sodium in Opalinus Clay, Environ. Sci. Technol. 41 (2007) 5002–5007. https://doi.org/10/bp2rtr.
[78] C.F. Gerald, Applied numerical analysis, Pearson Education India, 2004.
[79] K. Krabbenhøft, J. Krabbenhøft, Application of the Poisson–Nernst–Planck equations to the migration test, Cem. Concr. Res. 38 (2008) 77–88. https://doi.org/10/c7kjms.
[80] G.S. (1789-1854) A. du texte Ohm, Die galvanische Kette : mathematisch bearbeitet / von Dr. G. S. Ohm, T. H. Rieman, Berlin, 1827. http://gallica.bnf.fr/ark:/12148/bpt6k33646 (accessed March 21, 2018).
[81] R.A. Robinson, R.H. Stokes, R.G. Bates, Electrolyte solutions: The measurement and interpretation of conductance, chemical potential and diffusion in solutions of simple electrolytes, J. Electrochem. Soc. 107 (1960) 205C–206C.
[82] H.S. Harned, B.B. Owen, The physical chemistry of electrolytic solutions, (1939).
[83] G. Kirchhoff, Ueber die Auflösung der Gleichungen, auf welche man bei der Untersuchung der linearen Vertheilung galvanischer Ströme geführt wird, Ann. Phys. 148 (1847) 497–508.
[84] C.A.J. Appelo, A selection of publications, (2017). http://www.hydrochemistry.eu/pub/index.html.
[85] P. Blanc, X. Bourbon, A. Lassin, E.C. Gaucher, Chemical model for cement-based materials: Thermodynamic data assessment for phases other than C–S–H, Cem. Concr. Res. 40 (2010) 1360–1374.
[86] P. Blanc, P. Vieillard, H. Gailhanou, S. Gaboreau, N. Marty, F. Claret, B. Madé, E. Giffaut, ThermoChimie database developments in the framework of cement/clay interactions, Appl. Geochem. 55 (2015) 95–107. https://doi.org/10/f66gvq.
[87] E. Giffaut, M. Grivé, Ph. Blanc, Ph. Vieillard, E. Colàs, H. Gailhanou, S. Gaboreau, N. Marty, B. Madé, L. Duro, Andra thermodynamic database for performance assessment: ThermoChimie, Appl. Geochem. 49 (2014) 225–236. https://doi.org/10/f6n339.
[88] J. Diederik, L. Wang, E. Martens, D. Mallants, Thermodynamic database (CEMDATA07) for concrete in PHREEQC format, ResearchGate. (2013). https://www.researchgate.net/publication/237052766_Thermodynamic_database_CEMDATA07_for_concrete_in_PHREEQC_format (accessed April 6, 2018).
[89] S. Pradelle, M. Thiéry, V. Baroghel-Bouny, Sensitivity analysis of chloride ingress models: Case of concretes immersed in seawater, Constr. Build. Mater. 136 (2017) 44–56. https://doi.org/10/gc4pg2.
[90] S. Violet, S. Bejaoui, J.P. Ollivier, Microstructure et propriétés de transport des pâtes de ciment, CEA, France, 2005.
[91] P. Atkins, J. De Paula, Atkins' physical chemistry, N. Y. (2006) 77.